Progress In Electromagnetics Research C, Vol. 134, 131–141, 2023

Multi-Slot Antennas Excited by Novel Dual-Stub Loaded Microstrip Lines for 4G/5G Bands

Muhammad M. Hossain, M. M. Reazul Haque Tanmoy, and Saeed I. Latif*

Abstract—This paper presents a low-profile, stub-loaded multi-slot antenna that operates across 850 MHz to 4500 MHz. Remarkably, the new design meets the call of covering wideband frequencies used by many 4G and 5G New Radio bands from UHF to C bands. The antenna consists of two wide slots on the ground plane. Each slot comprises a straight segment connected to a larger circular slot. A novel microstrip feed line loaded with dual circular stubs excites the multi-slot antenna. The slots and feed lines are printed on each side of the dielectric substrate. This novel design offers pattern diversion capacity based on port excitation. Two prototypes were fabricated and tested to verify multiple simulation results including bandwidth, isolation, and group delays. A close consistency of measured and simulated results validates the design. Concurrently, good isolation between ports and nearly omnidirectional gain patterns are observed over the band. Further, the form factor of the proposed antenna makes it a suitable solution for modern 4G and 5G handheld devices.

1. INTRODUCTION

The evolution of wireless communication standards from global system for mobile communication (GSM) to 4G/long term evolution (LTE) and now to 5G offers significantly improved data rate for hand-held devices, such as smartphones, tablets, and smart watches. The emergence of new services, e.g., video calls, live video game streaming, and live traffic updates, have pushed the demand for novel infrastructure and technology which can handle higher data rate. New wireless standard releases suggest new approaches where huge number of smart devices are connecting millions of consumers across the globe at various frequencies [1]. To accommodate multiple 4G/LTE bands ranging from 800 MHz to 3800 MHz and newly proposed 5G bands up to 4500 MHz, antennas are needed with reasonably small dimensions and capable of covering the new spectrums. New wireless standards, such as LTE, desire to utilize the multi-path effects employing multiple antennas [2, 3] to reduce the multi-path loss and increase the data rate, essentially using the multiple-input multiple-output (MIMO) feature.

To support various hand-held devices, e.g., smartphones, tablets, laptops, and smart watches, advanced and efficient antennas are experiencing tremendous investigation in terms of size and dimensions. A common choice for these devices or the LTE base stations is the planar monopoles made of meandered strips, planar Inverted-F antennas (PIFAs), low profile printed microstrip antennas, and slot-based antennas [4–17]. Traditionally in many antennae designs compatible to LTE technology, two or more antenna elements are employed to achieve dual band operations where one element is responsible for the lower band of operation, and the other element takes care of the upper bands of 4G. Ref. [4] demonstrates a dual band antenna for the LTE band, which exploits the outer ring for the lower band (550 MHz) while for the upper band (2.9–3.5 GHz) another metamaterial structure near the feedline is used. In [5], a low profile electronically reconfigurable circular patch array is presented, where radio frequency switches are used to control antenna radiation characteristics. [6] reports a dual-band

Received 10 May 2023, Accepted 22 June 2023, Scheduled 5 July 2023
* Corresponding author: Saeed I. Latif (slatif@southalabama.edu).
The authors are with the Department of Electrical and Computer Engineering, University of South Alabama Mobile, AL 36688, USA.

MIMO antenna using four U-slit etched PIFAs and four L-slit etched PIFAs together, which operates at two frequency bands (2.6–2.8 and 3.4–3.6 GHz) with improved isolation for LTE mobile terminals. Using multi-branch monopole, dual band operation is demonstrated in [7] for LTE applications. Also, a monopole antenna with a parasitic patch [9] can provide coverage both at the upper and at the lower bands of the LTE technology. A dual band antenna, where a 'double G' textile coplanar waveguide (CPW)-fed monopole is used in [11], provides 2.4–2.7 GHz and 5.1–5.875 GHz of operation for MIMO application. Several works referring to [13, 14] are reported on low profile wideband monopole antennas, where hook and substrate integrated waveguide (SIW) resonator-based monopole antennas offer the coverage only for upper bands of 4G/LTE above 2000 MHz. [15] presents an antenna covering two bands (3.3 to 3.8 GHz and 4.8 to 5 GHz) from 5G communication, and it incorporates two double-oval-shaped dipoles, two double-oval-shaped feeding lines, and a cavity reflector. In [16], two of the LTE bands are covered, band 42 (3400–3600 MHz) and LTE band 46 (5150–5925 MHz), and this work presents an L shaped slot. A metamaterial based antenna in [17] demonstrates a dual band operation in LTE technology with a potential application in Ka-band and WLAN wireless standards.

This paper documents an ultra-wideband (UWB) low-profile antenna using open wide slot techniques targeting 4G and newly proposed 5G wireless systems. Two open and wide slots are used at the lengthwise edges of the ground plane and excited by a 50-Ω printed feed line. This technique excites and exploits a set of modes that merge respective resonances to maintain stable matching over a wideband of frequencies [18–22]. A new class of double circular stubs loaded feed line is introduced to shoot up the electromagnetic coupling from the feed line to multiple slots improving the overall bandwidth. The proposed antenna operates for UWB frequencies from 850 MHz to 4500 MHz (5.3:1), covering almost all the LTE bands including LTE 44 (700 L-band), LTE 34 (2000 L-band), LTE 42-43 (3500 L-band), and LTE 48-49 (3500 L-band). Additionally, it also covers 1850–1910/1930–1990 MHz (Personal Communications Service — PCS Band), and 1710–1755/2110–2155 MHz (Advanced Wireless Services — AWS Band). This increased range of frequencies is not covered by the previously reported dual stubs-based slot antennas [23, 24]. Remarkably, this antenna covers the newly released 5G new radio (NR) frequency bands: n77 to n79 frequency bands, beyond the 4G/LTE frequencies. [25–28] discuss several antenna designs for these newly allocated frequency bands for 5G NR bands where PIFA-based or printed designs are incorporated with array antennas to accommodate the new bands. This extended frequency coverage of both the 4G and 5G NR bands makes this proposed antenna very desirable in the case of switching between 4G and 5G systems as more mobile operators deploy new 5G wireless systems, and existing 4G/LTE systems are still in operation.

In the LTE base station antenna technology, application in the automotive and base station, several reported designs [29–32] introduced perpendicular elements to achieve pattern/polarization diversity. Still, this is quite challenging in low-profile antennas for handheld devices due to limited space. In the proposed design, pattern diversity is achieved by exciting two complementary sets of slots at the two lengthwise edges of the ground plane, like [24]. Multiple slots are excited for this purpose with a consistent measured port isolation below −18.5 dB over the entire frequency band of operation.

The communication is organized as follows. Section 2 introduces multi-slot antenna geometry with a double stubs-based feed network. The fabricated antenna results are presented in Section 3. Radiation pattern performance is analyzed in Section 4, where diversity performance is discussed. A comprehensive comparative study on radiation patterns from two different electromagnetic (EM) simulation software packages: Ansys HFSS, version 19, and CST microwave studio, are also presented in this section. Bandwidth definition of $S_{11} = -6$ dB (VSWR = 3) is considered as the design specification in this paper, which is widely used [8, 9, 14, 16].

2. DUAL STUBS LOADED MULTI-SLOT ANTENNA GEOMETRY

As depicted in Fig. 1, the multi-slot antenna consists of a wide straight slot cut into the ground plane, where the slot (L) is along the y-axis. One end of the straight slot is kept open, while the other end is connected to a circular slot of diameter 'R'. Two of these slots are placed in a complementary configuration as shown in the figure. Both slots are excited by planar feed lines that are printed on the flipside of the grounded dielectric substrate. Rogers TMM4 (relative permittivity $\varepsilon_r = 4.5$ and thickness = 3.175 mm) is used as the dielectric material.

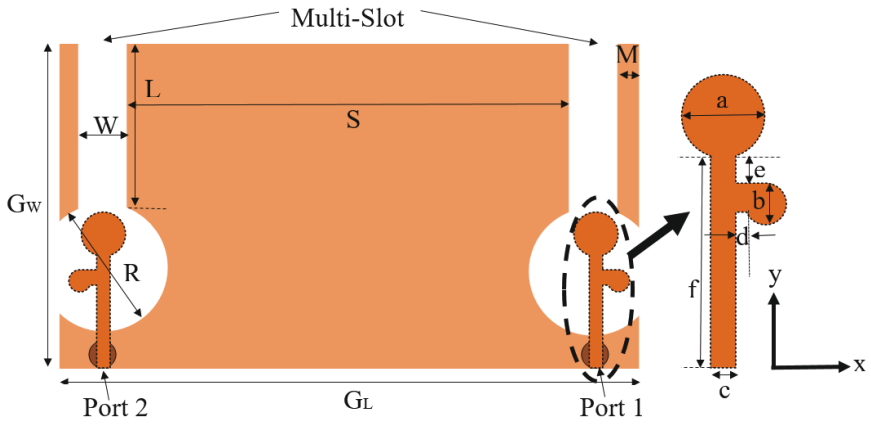

Figure 1. Proposed antenna geometry, indicating slot and stubs geometries.

A new class of stub loaded feed network is designed to excite each slot functionally. The primary feedline (f) is matched to two circular stubs at the center of the circular slot. A 50-Ω SMA connector excites the feed line. Fig. 1 depicts this novel feed line, and all parameters are summarized in Table 1. The circular stub over L slot has a segment with radius a. The other segment extends from the feed line (or from the center of the circular slot) to the $+x$ direction and has a circular stub with radius b. Both the rectangular stubs and the feed line have 50-Ω characteristic impedance width, which is 4.5 mm for this design.

Table 1. Antenna dimensions for the dual stub-loaded multi-slot antenna.

Antenna Parameters	G_W	G_L	W	R	S	M	a	b	c	d	e	f
Values (mm)	90	160	12	15	115	9	10	5.6	3	1.8	3.4	36

Primarily slot lengths were chosen for $\sim 3:1$ frequency bandwidth (850 MHz to 2600 MHz) of $S_{11} < -6$ dB. Thus, the first set of feed line parameters was chosen to excite each slot's lowest order or dominant mode. These already achieve a wide frequency band of operation. With the use of circular stubs, the bandwidth is further extended to cover the new 5G n77 to n79 bands. In simulations, a ground plane size of 160 mm ($= G_L$) × 90 mm ($= G_W$) is used. For wide-screen handheld devices, a broader ground plane is well-suited [24].

3. RESULTS AND DISCUSSIONS

A rigorous parametric study on slot dimensions and feed stubs is done to cover most of the LTE bands and new 5G NR n77 to n79 bands. The use of circular tuning stubs with the feed line significantly increases the impedance bandwidth due to the smoothness of the structure. Also, a few other appropriate antenna geometry variables are tabulated in Table 1. The placement of stub-loaded feed lines at the farthest edges of antenna ground resulted in good port isolation.

The overall antenna dimension as well as the dielectric substrate size is 140 mm × 80 mm. Fig. 2(a) and Fig. 2(b) show the top and bottom sides of the assembled antenna, respectively. The fabricated antenna's S-parameters were tested by an Anritsu 37369A Vector Network Analyzer (VNA). Simulated S_{11} frequency plots from CST Microwave Studio and Ansys HFSS are compared with the measured one in Fig. 2(c). A good agreement between measured and simulated port reflection data validates antenna's wideband impedance matching characteristics. As shown in Fig. 1(b), the $S_{11} < -6$ dB bandwidth of this proposed antenna is around 136.3% or 5.3:1 (820 MHz to 4335 MHz), and the measured bandwidth

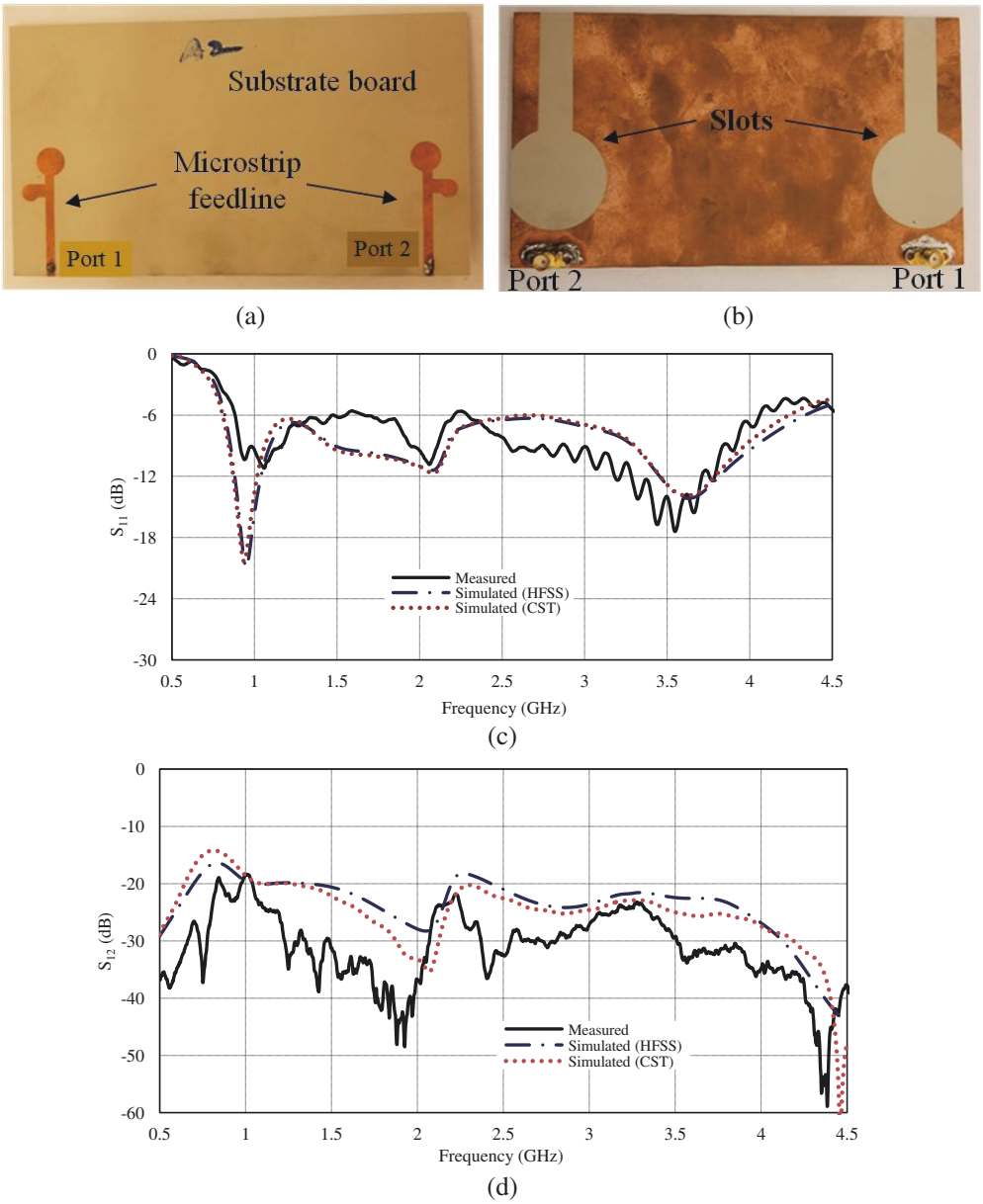

Figure 2. (a) Fabricated antenna prototype top view showing slotted ground plane. (b) Fabricated antenna prototype bottom view showing novel feed lines. (c) Simulated and measured S_{11} (dB), and (d) simulated and measured S_{12} (dB).

is 133.3% or 5:1 (820.3 MHz to 4100 MHz). The plot for S_{22} is very similar to S_{11} and is not shown in this figure. The isolation between ports is compared in Fig. 2(d), and an isolation below -18.6 dB can be noticed for the bandwidth without any additional decoupling elements. While in [24], two complementary slots are placed at two corners along the shorter side of a rectangular board, in this paper the slots are placed at two corners along the longer side, which has introduced an additional separation between ports. Along with the added physical separation, the use of circular stubs offers a significant improvement in isolation and bandwidth.

Surface current distributions at lower and center frequencies (1 GHz and 2.5 GHz) are shown in Figs. 3 and 4 for each port. The highest current magnitude at the excited slot edge enables primary electromagnetic radiation from this antenna.

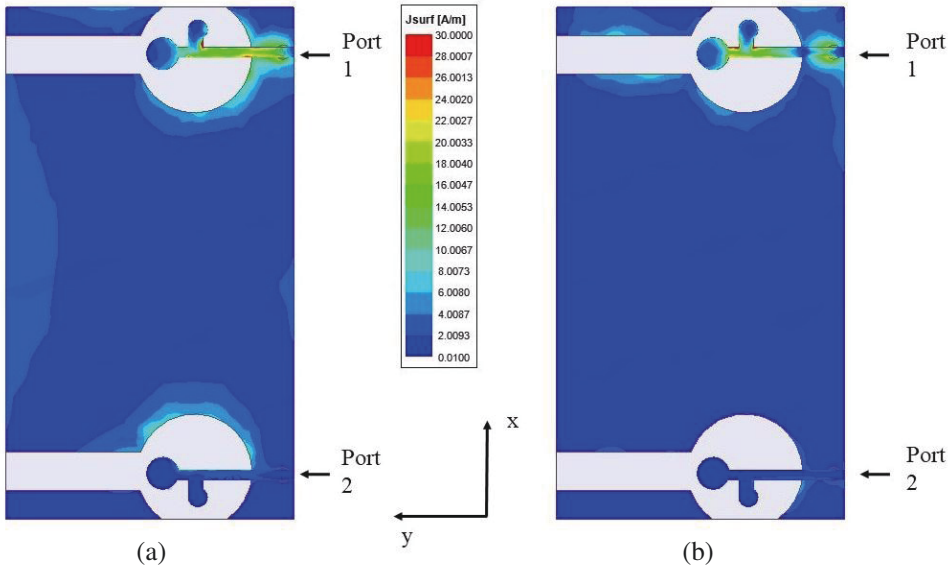

Figure 3. Ground plane and feed line surface current distributions (magnitude) of the proposed antenna at (a) 1 GHz and (b) 2.5 GHz, [port 1 excited and port 2 terminated].

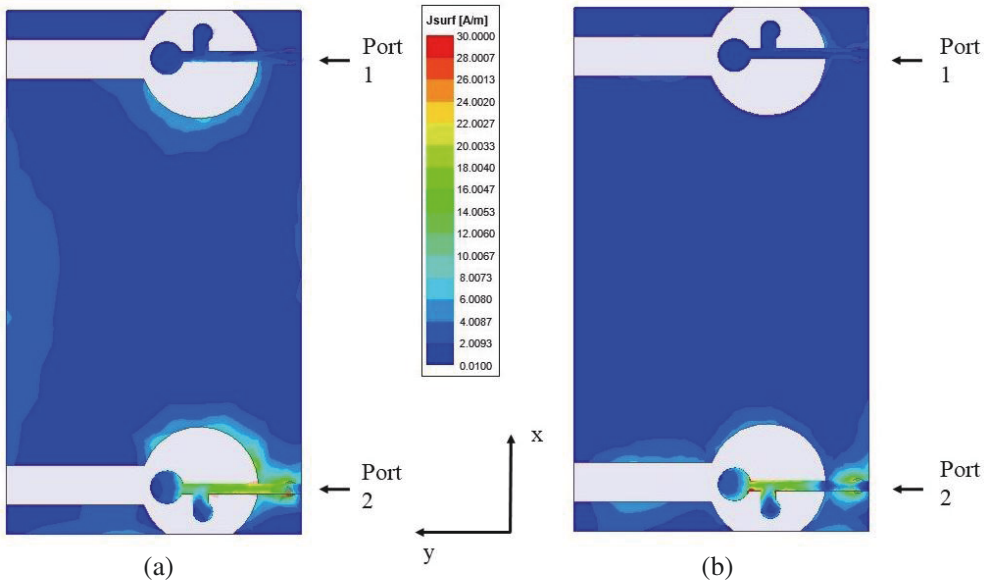

Figure 4. Ground plane and feed line surface current distributions (magnitude) of the proposed multi-sot slot antenna at (a) 1 GHz and (b) 2.5 GHz, with port 2 excited and port 1 terminated in a 50-Ω load.

4. RADIATION PATTERNS OF THE ANTENNA

Pattern diversity is realized through two reciprocal slots placed on the two lengthwise edges of the ground plane. Radiation patterns in the $\phi = 45°$ and $\phi = 135°$ planes are observed, where the patterns are significant because each slot consists of a straight slot and a circular slot at an orthogonal configuration excited by a feedline with orthogonal stubs at the end. Simulated radiation patterns are plotted in Fig. 5 at two different frequencies within the band in these two principal cuts. The figures on the left are when the port 1 is excited (on the left side in Fig. 2(b), and the right feedline (port 2) is terminated

with 50-Ω broadband load, and vice versa for radiation plots on the right side (port 2 excited, and port 1 terminated). From the radiation patterns at 1 GHz, it is evident that E_ϕ is the co-polarization component which has a nearly omnidirectional coverage in the $\phi = 45°$ and $\phi = 135°$, when port 1 and port 2 are excited, respectively. E_ϕ is the co-polarization component for the similar port excitations at a higher frequency, e.g., 3.5 GHz, but it becomes more directive. The antenna demonstrates nearly omnidirectional coverage by alternatingly exciting port 1 and port 2 with E_ϕ as the co-polarization component in both planes. It provides a peak gain of 4 dBi from $\theta = -180°$ to $0°$ when one port is excited and the other terminated in a 50-Ω load in both principal planes. In order to validate the simulated radiation patterns obtained from HFSS, the antenna is simulated in CST Microwave Studio and compared in Fig. 5. The results are in excellent agreement in both planes for various port

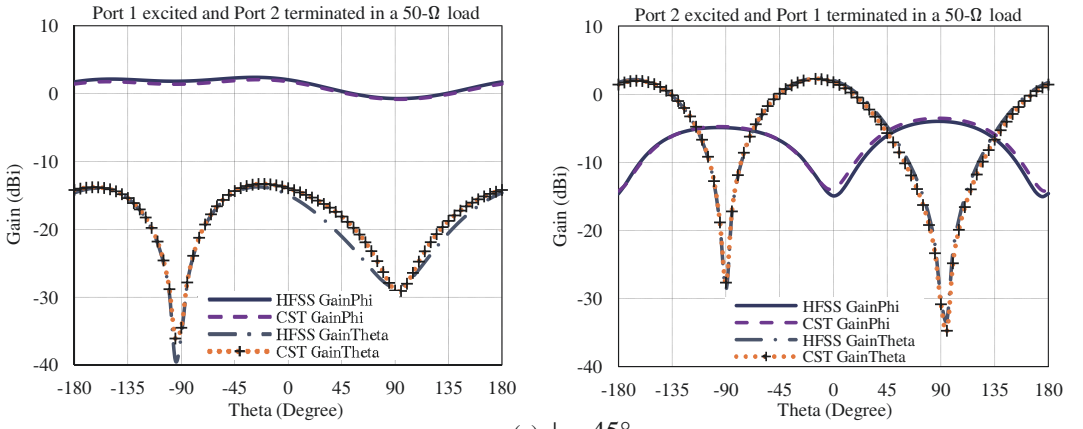

(a) $\phi = 45°$

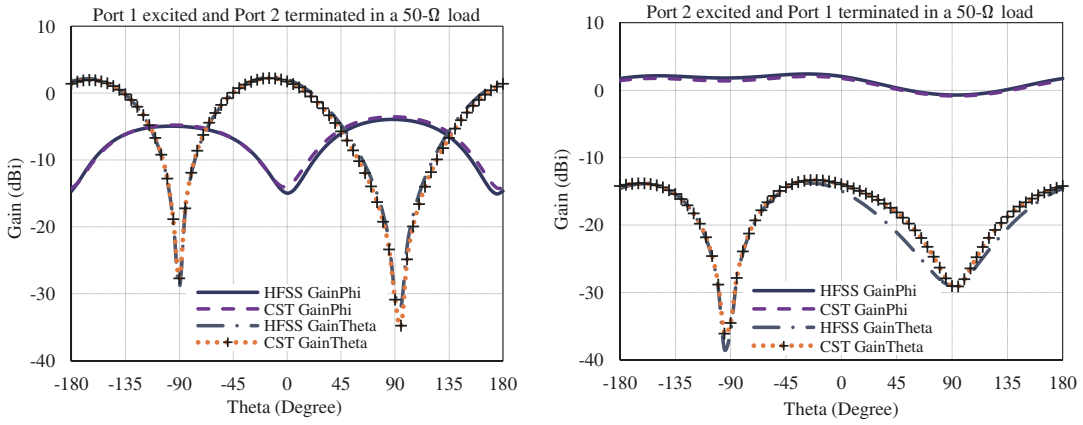

(b) $\phi = 135°$

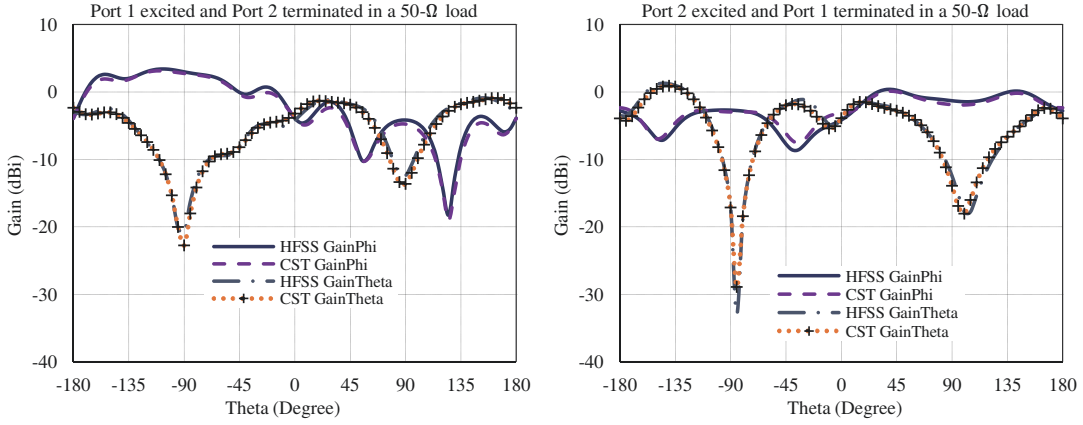

(c) $\phi = 45°$

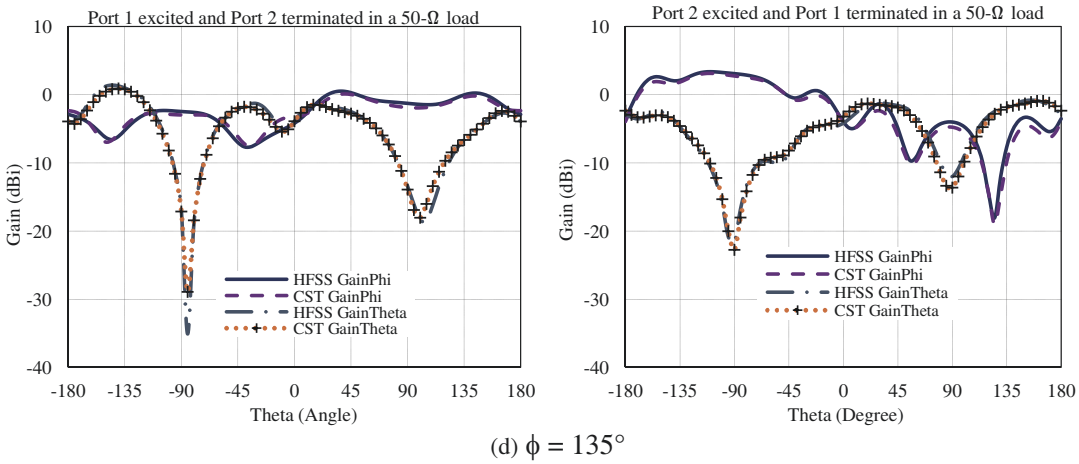

Figure 5. Gain pattern comparison of the antenna using Ansys HFSS and CST Microwave Studio: at 1 GHz in the (a) $\phi = 45°$ and (b) $\phi = 135°$ planes, and at 3.5 GHz in the (c) $\phi = 45°$ and (d) $\phi = 135°$ planes. (a) $\phi = 45°$, (b) $\phi = 135°$, (c) $\phi = 45°$, (d) $\phi = 135°$.

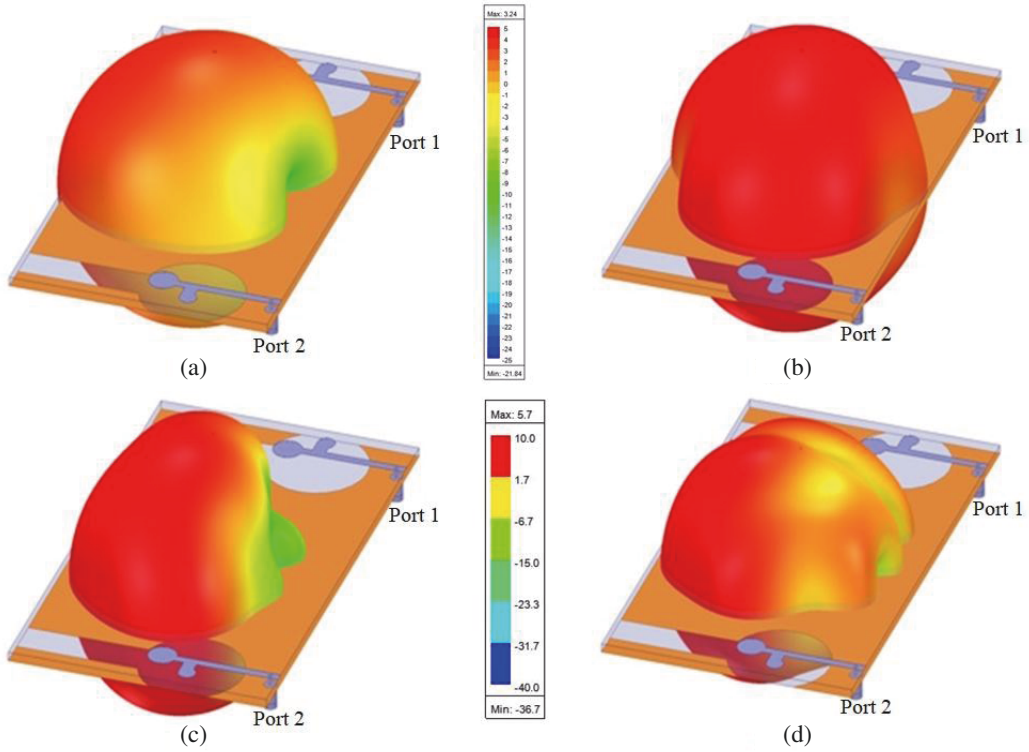

Figure 6. Plotted 3D Radiation patterns of the proposed antenna using Ansys HFSS at 1 GHz (a) when Port 1 is excited and Port 2 is terminated in a 50-Ω load and (b) when Port 2 is excited and Port 1 is terminated in a 50-Ω load, and at 2.5 GHz (c) when Port 1 is excited and Port 2 is terminated in a 50-Ω load and (d) when Port 2 is excited and Port 1 is terminated in a 50-Ω load.

excitations, as can be noticed in the figure. Each slot provides peak radiation related to its surface current magnitude. Thus, the antenna radiates toward $\theta = 90°$ direction (with respect to the z-axis) when port 1 is excited. Reciprocally, it radiates toward $\theta = -90°$ direction when port 2 is excited. Simulated 3D radiation patterns shown in Fig. 6 confirm the claim. This advantageous characteristic is the key to achieve pattern diversity from this type of antenna configuration with orthogonal feedings.

5. DIVERSITY PERFORMANCE

Pattern diversity of an antenna can be estimated through correlation coefficient (ρ) calculation, using scattering parameters data and radiation efficiency [33]. For 4G technology, a numeric value of less than 0.3 for the correlation coefficient ensures diversity performance [34]. The simulated correlation coefficient for the entire bandwidth is presented in Fig. 7, where it is evident that this value is equal to or less than 0.05 up to 3.3 GHz and below or around 0.2 above this frequency. This clearly indicates that signals from two ports do not vary together when being excited and allow acceptable diversity performance over the entire frequency of operation.

Further, the antenna group delay simulation result was validated using two identical fabricated multi-slot antennas. Two antennas declared as the transmitter antenna and receiver antenna were placed against each other and connected to the ports of the VNA in the lab. A displacement of 50 cm was maintained among the two antennas. Fig. 8 presents the software-generated simulated group delay on the top of the group delay plot calculated from the real-time measurement. Less than 4 ns variation in group delay is observed comparing the measured and simulated plots. The difference in the simulated

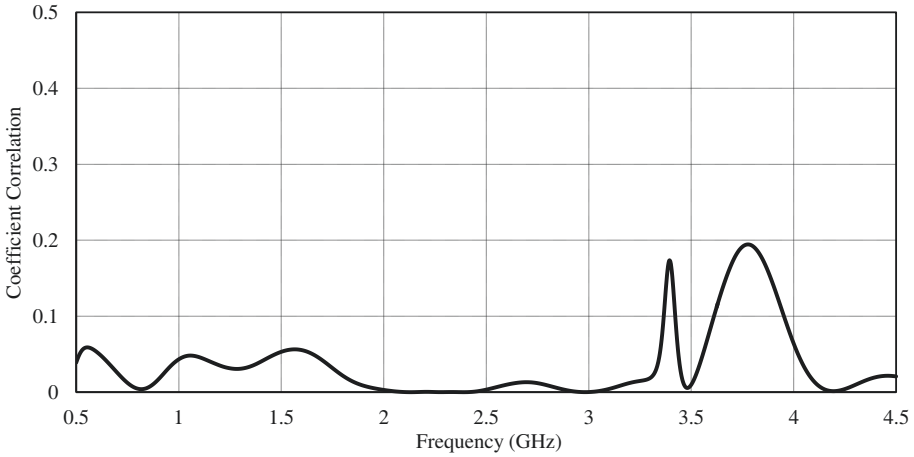

Figure 7. Calculated Correlation Coefficient (ρ) using simulated the S-parameters.

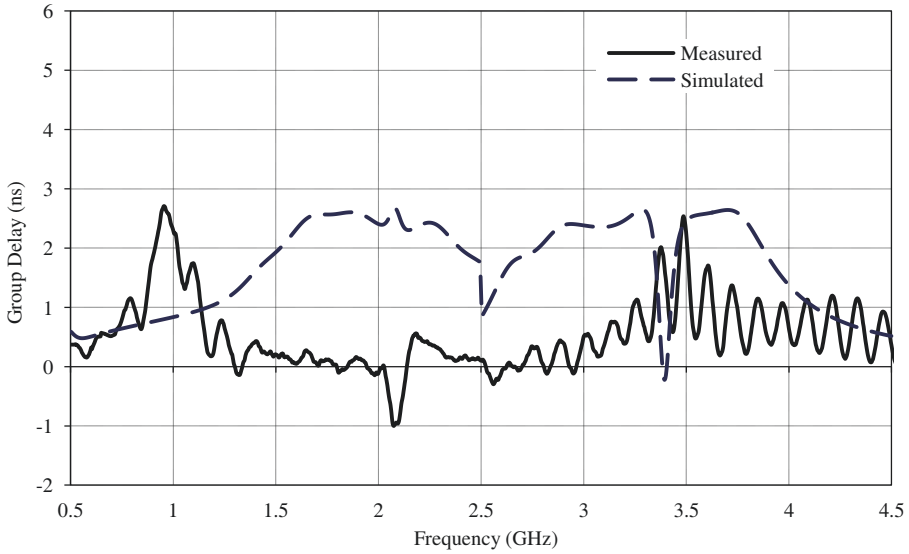

Figure 8. Simulated and measured group delay at 50 cm (both the antennas' Port 1 were excited while two port 2 were terminated in two 50-Ω load).

and measured group delays can be characterized by reflections from the surrounding objects causing ripples in the measured data. The measuring test environment setup followed a connection as port 1 of both antennas was excited and port 2 terminated in a 50-Ω matched load. The second data set was collected while port 2 of both antennas was excited and port 1 terminated. The generated data were close, and therefore only one is shown in the figure. Both the simulated and measured group delays are within 4 ns, and they have an average variation of 2 ns. For measurements, VNA cables add some discrepancies. This confirms the antenna's stable group delay or phase linearity performance.

6. CONCLUSION

We presented a multi-slot antenna employing a novel stub-loaded micro-strip feed line for 4G/5G applications. The multi-slots are composed of reciprocal straight and circular slots. Notably, the optimized antenna covers most of the LTE frequency bands from 850 MHz to 4500 MHz including PCS MHz and AWS bands, and newly released 5G NR bands, such as n77 (3300–4200 MHz) and n78 (3300–3800 MHz). Placing two reciprocal slots on two lengthwise edges of a ground plane allows radiation with pattern diversity suitable for UWB operation. The antenna was first designed and simulated in Ansys HFSS, a finite element method based electromagnetic solver. Later, the simulated results were confirmed through fabricated prototype measurement and CST Microwave Studio (uses method of moments (MOM) technique). A UWB performance with 5.3:1 impedance bandwidth and a simple pattern diversity capability make this antenna a standard solution to the modern LTE and 5G NR wireless industry.

ACKNOWLEDGMENT

The authors would like to thank Taylor E. Moat for the simulation and modeling of the antenna. The authors would like to acknowledge the support provided by the National Science Foundation (Award Number: 1833016) and Alabama Commission on Higher Education (ACHE) for partially funding this project.

REFERENCES

1. Selinis, I., K. Katsaros, M. Allayioti, S. Vahid, and R. Tafazoll, "The race to 5G era; LTE and Wi-Fi," *IEEE Access*, Vol. 6, 56598–56636, 2018, doi: 10.1109/ACCESS.2018.2867729.
2. Simon, J., S. M. Shyni, E. A. E. Jebaseeli, and G. Janakiraman, "Design of massive MIMO dual band antenna for 5G cellular mobile communication," *2020 4th International Conference on Electronics, Communication and Aerospace Technology (ICECA)*, 586–591, 2020, doi: 10.1109/ICECA49313.2020.9297409.
3. Hastürkoğlu, S., M. Almarashli, and S. Lindenmeie, "A compact wideband terrestial MIMO-antenna set for 4G, 5G, WLAN and V2X and evaluation of its LTE-performance in an urban region," *2019 13th European Conference on Antennas and Propagation (EuCAP)*, 1–5, 2019.
4. Hasan, M. M., M. R. I. Faruque, and M. T. Islam, "Dual band metamaterial antenna for LTE/bluetooth/WiMAX system," *Sci. Rep.*, Vol. 8, 1240, 2018, https://doi.org/10.1038/s41598-018-19705-3.
5. Donelli, M. and P. Febvre, "An inexpensive reconfigurable planar array for Wi-Fi applications," *Progress In Electromagnetics Research C*, Vol. 28, 71–81, 2012.
6. Li, G., H. Zhai, Z. Ma, C. Liang, R. Yu, and S. Liu, "Isolation-improved dual-band MIMO antenna array for LTE/WiMAX mobile terminals," *IEEE Antennas and Wireless Propagation Letters*, Vol. 13, 1128–1131, 2014, doi: 10.1109/LAWP.2014.2330065.
7. Cheng, T., J. Tsai, W. Hung, and S. Chen, "Dual-band handset antenna based on multi-branch monopole for LTE/WWAN applications," *2016 International Symposium on Antennas and Propagation (ISAP)*, 24–25, Okinawa, Japan, 2016.

8. Moriyama, T., M. Manekiya, and M. Donelli, "A compact switched-beam planar antenna array for wireless sensors operating at Wi-Fi band," *Progress In Electromagnetics Research C*, Vol. 83, 137–145, 2018.
9. Tsai, C. and K. Wong, "Combined-type dual-wideband and triple-wideband LTE antennas for the tablet device," *2015 IEEE 4th Asia-Pacific Conference on Antennas and Propagation (APCAP)*, 411–412, 2015, doi: 10.1109/APCAP.2015.7374426.
10. Bhardwaj, S. and Y. Rahmat-Sami, "C-shaped, E-shaped and U-slotted patch antennas: Size, bandwidth and cross-polarization characterizations," *2012 6th European Conference on Antennas and Propagation (EUCAP)*, 1674–1677, 2012, doi: 10.1109/EuCAP.2012.6206679.
11. Zhang, Y., H. Jin, and C. M. Li, "A compact dual-wideband monopole antenna with parasitic patch for 2G/3G/LTE/WLAN/WiMAX applications," *2017 IEEE 5th International Symposium on Electromagnetic Compatibility (EMC-Beijing)*, 1–4, 2017, doi: 10.1109/EMC-B.2017.8260438.
12. Mantash, M., S. Collardey, A. Tarot, and A. Press, "Dual-band WiFi and 4G LTE textile antenna," *2013 7th European Conference on Antennas and Propagation (EuCAP)*, 422–425, Gothenburg, Sweden, 2013.
13. Menon, S. K., G. Marchi, M. Donelli, M. Manekiya, and V. Mulloni, "Design of an ultra wide band antenna based on a siw resonator," *Progress In Electromagnetic Research C*, Vol. 103, 187–193, 2020.
14. Robol, F. and M. Donelli, "Circularly polarized monopole hook antenna for ISM-band systems," *Microwave and Optical Technology Letters*, Vol. 60, No. 6, 2018.
15. Hua, Q., Y. Huang, A. Alieldin, C. Song, T. Jia, and X. Zhu, "A dual-band dual-polarized base station antenna using a novel feeding structure for 5G communications," *IEEE Access*, Vol. 8, 63710–63717, 2020, doi: 10.1109/ACCESS.2020.2984199.
16. Li, J., X. Zhang, et al., "Dual-band eight-antenna array design for MIMO applications in 5G mobile terminals," *IEEE Access*, Vol. 7, 71636–71644, 2019, doi: 10.1109/ACCESS.2019.2908969.
17. Asif, M., D. A. Sehrai, S. H. Kiani, et al., "Design of a dual band SNG metamaterial based antenna for LTE 46/WLAN and Ka-band applications," *IEEE Access*, Vol. 9, 71553–71562, 2021, doi: 10.1109/ACCESS.2021.3077844.
18. Tanmoy, M. M. R. H., S. I. Latif, A. T. Almutawa, F. Capolino, and M. M. Hossain, "Wide gain-bandwidth from an ultrathin high impedance surface-based leaky wave antenna using multi-feed excitation," *2020 Southeast Con.*, 1–2, 2020, doi: 10.1109/SoutheastCon44009.2020.9249724.
19. Yao, Y. and Z. Feng, "A novel band-notched ultra-wideband microstrip-line fed wide-slot antenna," *2006 Asia-Pacific Microwave Conference*, 1976–1978, 2006, doi: 10.1109/APMC.2006.4429795.
20. Reazul Haque Tanmoy, M. M., S. I. Latif, A. T. Almutawa, and F. Capolino, "Small-scale beam scanning with an ultrathin high impedance surface-based leaky wave antenna with multiple feeds," *2020 IEEE/MTT-S International Microwave Symposium (IMS)*, 17–20, Los Angeles, CA, USA, 2020, doi: 10.1109/IMS30576.2020.9223801.
21. Hossain, M. M., S. I. Latif, and E. A. Spencer, "Hybrid perturbations in stacked patch-ring circularly polarized microstrip antennas for CubeSat applications," *IEEE Aerospace and Electronic Systems Magazine*, Vol. 37, No. 3, 24–31, March 1, 2022, doi: 10.1109/MAES.2022.3141436.
22. Kulkarni, A. N. and S. K. Sharma, "Frequency reconfigurable microstrip loop antenna covering LTE bands with MIMO implementation and wideband microstrip slot antenna all for portable wireless DTV media player," *IEEE Transactions on Antennas and Propagation*, Vol. 61, No. 2, 964–968, Feb. 2013, doi: 10.1109/TAP.2012.2223433.
23. Henderson, K. Q., S. I. Latif, G. Lazarou, S. K. Sharma, A. Tabbal, and S. Saial, "Dual-stub loaded microstrip line-fed multi-slot printed antenna for LTE bands," *2018 IEEE International Symposium on Antennas and Propagation & USNC/URSI National Radio Science Meeting*, 1743–1744, 2018, doi: 10.1109/APUSNCURSINRSM.2018.8608453.
24. Henderson, K. Q., S. I. Latif, G. Y. Lazarou, S. K. Sharma, and A. Tabbal, "Multi-slot antennas excited by novel dual-stub loaded microstrip lines for 4G LTE bands," *Progress In Electromagnetics Research M*, Vol. 75, 1–12, 2018.

25. Yuan, X.-T., Z. Chen, T. Gu, and T. Yuan, "A wideband PIFA-pair-based MIMO antenna for 5G smartphones," *IEEE Antennas and Wireless Propagation Letters*, Vol. 20, No. 3, 371–375, Mar. 2021, doi: 10.1109/LAWP.2021.3050337.
26. Sim, C., H. Liu, and C. Huang, "Wideband MIMO antenna array design for future mobile devices operating in the 5G NR frequency bands n77/n78/n79 and LTE band 46," *IEEE Antennas and Wireless Propagation Letters*, Vol. 19, No. 1, 74–78, Jan. 2020, doi: 10.1109/LAWP.2019.2953334.
27. Hossain, M. M., M. J. Alam, and S. I. Latif, "Orthogonal printed microstrip antenna arrays for 5G millimeter-wave applications," *Micromachines*, Vol. 13, No. 1, 53, 2022, https://doi.org/10.3390/mi13010053.
28. Zhao, A. and Z. Ren, "Wideband MIMO antenna systems based on coupled-loop antenna for 5G N77/N78/N79 applications in mobile terminals," *IEEE Access*, Vol. 7, 93761–93771, 2019, doi: 10.1109/ACCESS.2019.2913466.
29. Wolosinski, G., V. Fusco, and P. Rulikowski, "Mode-based MIMO antenna with polarization and pattern diversity for base station applications," *2018 IEEE International Symposium on Antennas and Propagation & USNC/URSI National Radio Science Meeting*, 493–494, 2018, doi: 10.1109/APUSNCURSINRSM.2018.8608704.
30. Park, S., V. Nguyen, and R. S. Aziz, "Multi-band, dual polarization, dual antennas for beam reconfigurable antenna system for small cell base station (Invited paper)," *2014 International Workshop on Antenna Technology: Small Antennas, Novel EM Structures and Materials, and Applications (iWAT)*, 159–160, 2014, doi: 10.1109/IWAT.2014.6958625.
31. Liu, H., Y. Liu, and S. Gong, "An ultra-wideband horizontally polarized omnidirectional connected vivaldi array antenna," *2016 International Symposium on Antennas and Propagation (ISAP)*, 798–799, 2016.
32. Kim, H., J. Jeon, M. K. Khattak, S. Kahng, S. Yoo, and E. Shin, "Design of a dual-band LTE MIMO antenna to be embedded in automotives," *2015 International Symposium on Antennas and Propagation (ISAP)*, 1–3, 2015.
33. Blanch, S., J. Romeu, and I. Corbella, "Exact representation of antenna system diversity performance from input parameter description," *Electron. Lett.*, Vol. 39, 705–707, 2003.
34. Sharawi, M. S., *Printed MIMO Antenna Engineering*, Artech House, Norwood, MA, USA, 2014.